Astron. Astrophys. 297, 727–738 (1995)

ASTRONOMY AND ASTROPHYSICS

Stellar evolution of low and intermediate-mass stars

I. Mass loss on the AGB and its consequences for stellar evolution

T. Blöcker*

Astrophysikalisches Institut Potsdam, Telegrafenberg A27, D-14473 Potsdam, Germany
e-mail: tbloecker@aip.de

Received 9 June 1994 / Accepted 22 October 1994

Abstract. We have performed extensive stellar evolution calculations for initial masses between 1 and $7M_{\odot}$ all the way from the main sequence through the AGB towards the stage of white dwarfs.

Mass loss has been taken into account with different descriptions for the RGB, AGB and post-AGB phase. On the AGB we considered mass loss with a formula based on dynamical calculations of the atmospheres of Mira-like stars. Our results are consistent with empirical initial-final mass relations.

It is shown that hot bottom burning and mass loss are closely connected. The overluminosity as well as the nucleosynthesis of hot bottom burning models can depend sensitively on mass loss.

Furthermore, we discuss the influence of mass loss on the internal structure reached at the tip of the AGB, and emphasize that post-AGB timescales will depend strongly on the AGB history, i.e. on the initial mass and the applied mass-loss law.

Key words: stars: evolution – stars: mass loss – stars: AGB, post-AGB

1. Introduction

The evidence of mass loss during the late stages of evolution has been known for a long time. Already in 1935 Adams and McCormack discovered blue shifted metal lines in the spectra of red giants. Deutsch (1956) derived mass-loss rates for the supergiant α Her from blue shifts of optical absorption lines. Later on, Reimers (1975) published his famous mass-loss law for red giants:

$$\dot{M} = 4 \cdot 10^{-13}\, \eta_{\rm R} \frac{LR}{M} \qquad [M_{\odot}/{\rm yr}] \qquad (1)$$

with $1/3 < \eta_{\rm R} < 3$ and L, R and M in solar units.
This rate gives a quite good mass-loss description for stars on the RGB and in the stage of central helium burning but is, in principle, not applicable for AGB stars when dust formation becomes important. According to Weidemann & Koester (1983) the upper mass limit for white-dwarf formation is $M_{\rm ZAMS} \approx 8M_{\odot}$. For such high masses the integrated mass loss amounts to only a few percent at the base of the AGB. Thus high mass losses must take place during the AGB evolution in order to remove the whole envelope before the core mass reaches the Chandrasekhar limit. In terms of the Reimers rate this would require al least $\eta_{\rm R} \approx 4.5$. But this is in contrast with the observed mass-loss rates of low mass stars for which a smaller $\eta_{\rm R}$ ($\lesssim 1$) is more suitable.

The quantitative determination of a mass-loss law on the AGB is a complex task. On the one hand, the derivation of mass-loss rates from observations corresponds often to single objects and not to the majority of the AGB population. Fits performed for a sample of objects suffer often from a large scatter of the observational properties. On the other hand, the detailed mechanism of mass loss is only poorly known up to now.

Typical members of the AGB are Mira and OH/IR stars which are long-period variables surrounded by circumstellar dust shells. In the case of the OH/IR stars these dust shells are optically thick, and the object is only visible in the infrared. By means of theoretical models and observations the structure of the circumstellar dust shells can provide information on mass loss. The corresponding observations are based on infrared transitions of silicates and carbides as well as on fluxes at wavelengths of 12, 25, 60 and 120μm. Furthermore, OH maser emissions and rotational and vibrational transitions of the CO molecule are often used.

The surveys of Neugebauer & Leighton (1969), Woolf & Ney (1969), Price & Walker (1976), Johannsson et al. (1977), Baud et al. (1979) and Knapp & Morris (1985) in the infrared and radio regime and especially the photometric and spectroscopic data of IRAS provided a lot of observational material. The mission of ISO will give further insights.

* *Former address:* Institut für Astronomie und Astrophysik, D-24098 Kiel, Germany

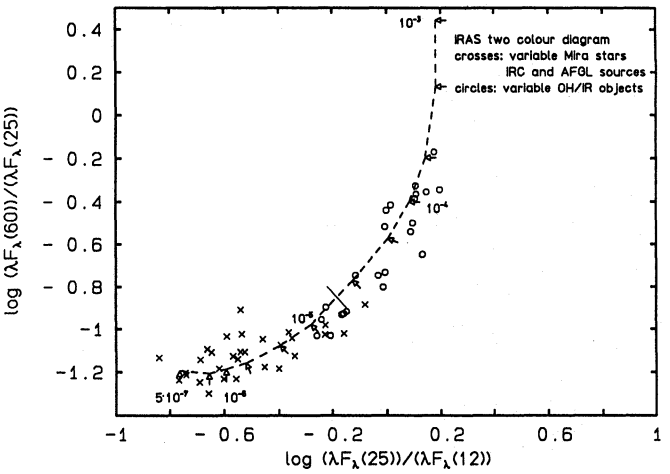

Fig. 1. Mass loss in the IRAS two colour diagram. $\lambda F_\lambda(x)$ is the wavelength times the flux density at x = 12, 25 und 60 μm. The dashed line indicate the colours of dust shells with different mass-loss rates according to Bedijn (1987) (cf. his Figs. 1a and 3a) The arrows denote mass-loss rates of (starting in the lower left corner) $2 \cdot 10^{-7}$, $5 \cdot 10^{-7}$, $1 \cdot 10^{-6}$, $2 \cdot 10^{-6}$, $5 \cdot 10^{-6}$, $1 \cdot 10^{-5}$, $2 \cdot 10^{-5}$, $5 \cdot 10^{-5}$, $1 \cdot 10^{-4}$, $2 \cdot 10^{-4}$, $5 \cdot 10^{-4}$, $1 \cdot 10^{-3}$ $M_\odot$/yr. At $\dot{M} \gtrsim 10^{-5} M_\odot$ the dust-shell silicate feature changes from emission to absorption and the shell gets optically thick (indicated by a line)

The observations show clearly that the silicate feature at 9.7μm changes with increasing optical depth of the dust shell from emission to absorption. This indicates that mass loss is increasing from the Mira towards the OH/IR phase. In the case of carbon-rich dust shells there exists a corresponding carbide feature at 11.2μm. One can also conclude from observed CO features that mass loss takes place all the way along the AGB (Kuiper et al. 1976).

Baud & Habing (1983) deduced from temporal correlations of OH and infrared fluxes that the OH maser should be saturated. Since a saturation of the maser is based on a thick dust shell and only ≈30% (Bowers 1985) of the Mira stars show maser emission one can again suppose that there exists an evolutionary connection from the Mira to the OH/IR phase. Finally, the non-variable OH/IR objects are interpreted as stars that have already left the AGB (Habing et al. 1987). Their mass loss rates are orders of magnitudes smaller than at the tip of the AGB (Bedijn 1987; van der Veen et al. 1989).

Figure 1 shows an IRAS two colour diagram for variable sources (adapted from Bedijn 1987). In such a diagram one can see a broad sequence from the Mira stars in the lower left to the OH/IR objects in the upper right part. The non-variable OH/IR sources lie on a quasi horizontal branch (not shown in Fig. 1, cf. Olnon et al. 1984). Dust shell calculations lead to the interpretation that the loci shown in Fig. 1 are mainly determined by the mass-loss rates which increase from the Mira towards the OH/IR phase (Rowan-Robinson et al. 1986; Bedijn 1987; Volk & Kwok 1988; Hashimoto et al. 1990; van der Veen 1987). Furthermore, these models indicate that mass loss should increase faster and faster along the AGB ("accelerated mass loss") in order to fit the observed dust shell spectra sufficiently well. Recent hydrodynamical calculations (Szczerba & Marten 1993a) confirm this general behaviour.

The physical mechanism of mass loss is not well understood up to now, and different approaches are discussed (cf. Lafon & Berruyer 1991), e.g., Alvèn waves or acoustic waves. However, shock and dust-driven winds seem to be the most promising scenario. In the case of dust-driven winds radiation pressure tranfers momentum to the dust. Then the dust accelerates the gas to escape velocity via collisions. Although the dust to gas mass ratio is low ($\approx 1/100$) the high opacity of the dust provides a high efficiency. Nevertheless, one problem arises: the dust condensation must take place in the immediate vicinity of the star but the densities at the condensation point ($T_{\rm cond} \approx 1000$ K) are rather low. However, due to the variability of AGB stars, pulsation-driven shock waves occur in the atmosphere. These shock waves increase the atmospheric scale height and, thus, the density at the condensation point. Indeed, the dynamical calculations of Bowen (1988) do show that only the combination of shock- and dust-driven winds leads to sufficiently high mass-loss rates. Without dust, mass loss decreases by two orders of magnitude.

The strength of the stellar winds along the AGB determine the duration of the AGB evolution which is terminated when the envelope mass is reduced to the order of several percent of the total stellar mass (i.e. to ≈ several $10^{-2} M_\odot$). Therefore, mass loss determines also the possible number of thermal pulses and therewith the nucleosynthesis connected with them. The internal structure reached at the tip of the AGB, i.e. the thermomechanical structure of the hydrogen-exhausted core, is also a function of the AGB mass-loss due to the increasing contraction and electron degeneracy of the core with increasing AGB lifetime. This has severe consequences for the subsequent evolution of central stars of planetary nebulae.

This paper is organized as follows: After presenting some computational details in Sect. 2 we discuss the treatment of mass loss during the late stages of stellar evolution, beginning with the RGB in Sect. 3.1. We will summarize some AGB mass-loss formulae in Sect. 3.2.1, deriving also a new formula. The results of our evolutionary calculations for different mass-loss formulae are given in Sect. 3.2.2. Furthermore, we discuss mass-loss modulations by thermal pulses (Sect. 3.2.3) and the connection between mass loss and hot bottom burning (Sect. 3.2.4) as well as the influence of mass loss on the internal structure reached at the tip of the AGB (Sect. 3.2.5). Finally, we summarize our results and give some conclusions (Sect. 4).

The second part of this series will be devoted to the post-AGB evolution of our models. Special attention will be paid to the fading part of the evolution and the treatment of mass loss (Blöcker 1994a) A detailed description of thermal-pulse properties and a discussion of hot bottom burning models will be given in the third part (Blöcker 1994b).

2. Computational details

We used the well-known Kippenhahn code in a widely modified and extended version of Schönberner's (1983) adaption (cf. Blöcker 1993a). Starting at the zero age main sequence (ZAMS) we have calculated the evolution of 1, 3, 4, 5 and $7 M_\odot$ stars through the AGB towards the stage of white dwarfs. The initial composition was $(X, Y, Z) = (0.739, 0.24, 0.021)$. Radiative opacities are based on the calculations of Cox & Stewart (1970) in order to be compatible with former calculations of Schönberner (1979, 1983) and Blöcker & Schönberner (1990, 1991) and to get a homogeneous set of evolutionary tracks. Work is in progress to re-calculate some representative tracks with the recent OPAL opacities (Rogers & Iglesias 1992; Iglesias et al. 1992) but we do not expect any significant changes to our conclusions. Conductive opacities have been taken from Hubbard & Lampe (1969) and Canuto (1970). Convection was treated within the mixing-length theory of Böhm-Vitense (1958) with a mixing length parameter of $\alpha = 1.5$ and 2, resp. The boundaries of convective regions have been determined with the Schwarzschild criterion. Overshooting, semiconvection or diffusion were not considered.

To achieve a reasonable numerical accuracy a typical evolved AGB model consists of up to 1800 mass shells. Time steps have not only been coupled to interior changes but have been also matched to the luminosity changes of the hydrogen and helium burning shell in order to provide a proper resolution of thermal-pulse cycles and of the fading part of the post-AGB evolution. An automatical adjustment of the fit mass (giving the mass fraction calculated with the Henyey method) guaranteed throughout the whole calculations a proper treatment of gravothermal energy contributions even in the very outer parts of the envelope. At the tip of the AGB typically only 1% of the envelope mass (i.e. $\approx 10^{-6} M_\odot$) or even less are not included in the Henyey method.

Mass loss has been taken into account since the beginning of the RGB. We followed for all initial masses the evolution towards the white dwarf stage with a common treatment of mass loss composed of different descriptions for the RGB, AGB and post-AGB phase. Additionally, we calculated some sequences on the AGB with other mass-loss formulae. The whole set of evolutionary calculations presented here and in the next parts of this series is based on $\approx 10^6$ stellar models.

3. Mass loss in late stages of stellar evolution

3.1. On the RGB

Already on the RGB mass loss can play an important role for low-mass models which suffer from the central helium-flash. More massive models are scarcely affected. We considered mass loss during the RGB stage and central helium burning according to the Reimers formula (1). Concerning the $1 M_\odot$ sequence we choose on the RGB $\eta_R = 0.5$ (cf. Maeder & Meynet 1989). Due to its long lifetime on the RGB the model lost $\approx 30\%$ of its initial mass. During central helium-burning mass losses are relatively small (1.2% of the initial mass) compared to the RGB phase because the luminosity is now much more smaller.

In the case of more massive models (3, 4, 5, $7 M_\odot$) we have set $\eta_R = 1$. For these models mass loss along the RGB is not important, their initial masses are reduced by only 1-3% until the beginning of the AGB.

During the subsequent AGB evolution the Reimers formula is not applicable any longer since it cannot reproduce the strong increase of the mass-loss rate.

3.2. On the AGB

3.2.1. Mass-loss formulae

In the following discussion and derivation of mass-loss formulae the η_R in the Reimers law is always set to unity and the stellar masses M, radii R and luminosities L are given in solar units.

In order to get a mass-loss law which is more consistent with the AGB evolution, Volk & Kwok (1988) considered the objection to the "evolutionary extrapolation" of the Reimers' rate mentioned above and introduced a modified formula

$$\dot{M}_{\rm VK} = 1.8 \cdot 10^{-12} \frac{M_{\rm ZAMS}}{8} \frac{LR}{M} \qquad [M_\odot/{\rm yr}], \tag{2}$$

which yields more adequate rates for different initial masses but collides with the observed inital-final mass relationship of Weidemann (1987) leading to too high final masses (cf. Fig. 4).

Bryan et al. (1990) improved this mass-loss description by introducing a term which is quadratic in the initial mass:

$$\dot{M}_{\rm BVK} = 1.15 \cdot 10^{-13} \eta_{\rm BVK} \frac{LR}{M} \qquad [M_\odot/{\rm yr}], \tag{3}$$

with

$$\eta_{\rm BVK} = M_{\rm ZAMS}^2 - 10.6 M_{\rm ZAMS} + 10.2. \tag{4}$$

The agreement with the initial-final mass relation is much better than in the previous case (see Fig. 4). However, for large initial masses the total mass loss seems to be still somewhat too small. Please note that the final masses provided by (2) and (3) are based on analytical estimations and have been taken from the respective publications.

The mass-loss formula of Bedijn (1987) yields final masses which are somewhere between the masses predicted by $\dot{M}_{\rm VK}$ and $\dot{M}_{\rm BVK}$ (for $M_{\rm ZAMS} < 6 M_\odot$) and does also not agree with the observed initial-final mass relation (cf. Bryan et al. 1990; Weidemann 1993).

Studying the statistical properties of OH/IR stars Baud & Habing (1983) established a relation between the OH luminosity of the maser emission and the mass-loss rate. Furthermore, they derived the mass-loss law

$$\dot{M}_{\rm BH} = 4 \cdot 10^{-13} \frac{M_{\rm e,0}}{M_{\rm e}} \frac{LR}{M} \qquad [M_\odot/{\rm yr}], \tag{5}$$

which differs from the Reimers rate due to the dependence on the actual envelope mass $M_{\rm e}$. $M_{\rm e,0}$ is the envelope mass at the beginning of the maser activity which is approximated by the

corresponding value at the base of the AGB. For most parts of the AGB (and $M > 2M_\odot$) $\dot{M}_{\rm BH} \approx \dot{M}_{\rm R}$ holds because $M_{\rm e}$ does not differ much from the stellar mass M. Only at the end of the AGB evolution is the envelope mass reduced to such an extent as to provide a steep increase of the mass-loss rates leading to much higher values than predicted by $\dot{M}_{\rm R}$ ("superwind phase", Renzini 1981). However, our calculations indicate that also this law is not consistent with the observed initial-final mass relationship. For instance, a $3M_\odot$ model finished its AGB evolution with a final mass of $0.814M_\odot$ (cf. Fig. 4).

Recently, Vassiliadis & Wood (1993) presented a mass-loss law which has been empirically coupled to the pulsational period P_0 (fundamental mode). They distinguish two phases depending on the value of P_0: If $P_0 < 500$ d the mass-loss rates are exponentially increasing with P_0: $\log \dot{M} = -11.4 + 0.0125 P_0$ (Wood 1990). For larger periods they assume a mass-loss according to the relation $\dot{M} = L/(c \cdot v_{\rm exp})$, corresponding to a maximum momentum tranfer of the photons by single scattering events. The expansion velocity $v_{\rm exp}$ of the stellar wind is given by a parametrization of Wood (1990).

However, for $M > 2.5M_\odot$ Vassiliadis & Wood (1993) had to scale down the exponential increase of their mass-loss rates in order to reach periods greater than 500 d. Finally, they got (upper case: $M \leq 2.5M_\odot$, lower case: $M > 2.5M_\odot$)

$$\dot{M}_{\rm VW} = \begin{cases} \min\left[\frac{L}{c}\frac{1}{v_{\rm exp}}, 10^{-11.4+0.0125\,P_0}\right] \\ \min\left[\frac{L}{c}\frac{1}{v_{\rm exp}}, 10^{-11.4+0.0125(P_0-100(M-2.5))}\right] \end{cases} \quad (6)$$

The corresponding final masses agree with the empirical relationship of Weidemann (1987) within $0.1M_\odot$ (Fig. 4).

It should be noted that, in general, the scattering, and thus $\dot{M}$, depends also on the optical depth τ (Salpeter 1974). In the case of optically thick envelopes (like those of OH/IR objects) the photons are scattered several times leading to an enhanced stored momentum in the envelope. Correspondingly, the mass-loss rate increases linearly with the mean optical depth leading to the conclusion that, as outlined by Netzer & Elitzur (1993), "to lowest order, radiation pressure does not provide any constraint on the mass-loss rate". We thus did not consider limiting mass-loss rates.

Bowen (1988) investigated the dynamical structure of long-period variable stars and calculated shock-driven winds in atmospheres of Mira-like stars. Such winds determine both the dynamical behaviour of the atmospheres and the mass loss. His calculations have been performed with and without the inclusion of dust and one major result was that only the combination of shock-driven winds and outer dust layers are able to provide typical AGB mass-loss rates. We have taken his models in order to construct a mass-loss formula which reflects the strong increase of mass loss during the AGB evolution, agrees with observed initial-final mass relationships, and is applicable to stellar evolution calculations (cf. Blöcker 1989,1993a).

First of all we had to make some restrictions. We considered only pulsations in the fundamental mode with periods P_0 calculated according to Ostlie & Cox (1986):

$$\log(P_0/{\rm d}) = -1.92 - 0.73 \log M + 1.86 \log R, \quad (7)$$

and took his standard model (that means e.g. $T_{\rm eff} = 3000$ K, piston velocity $v_{\rm p} = 3.5$ km/s, dust condensation at $T_{\rm cond} = 1500$ K, for more details see Bowen 1988) for stellar masses of 1.0, 1.2, 1.6 and $2.0M_\odot$. As discussed above the luminosity seems to be the major parameter concerning the strong increase of the mass loss during the AGB evolution. Therefore, we correlated Bowen's mass-loss rates $\dot{M}_{\rm B}$ directly with the luminosity, and found in terms of $\dot{M}_{\rm R}$

$$\dot{M}_{\rm B} \sim \eta(L) \cdot \dot{M}_{\rm R}, \quad (8)$$

with a luminosity dependent function $\eta(L)$. Because the mass-loss rates increase so strongly when the star climbs up the AGB, i.e. when the luminosity rises, we assumed

$$\eta(L) \sim L^x. \quad (9)$$

Performing this for *each mass* we evaluated the respective exponents x (with correlation coefficients ≥ 0.98), which in turn are lying in a narrow intervall of $2.46 \leq x \leq 2.88$. Taking the mean $\overline{x} = 2.7$ we got

$$\dot{M}_{\rm B} \sim L^{2.7} \cdot \dot{M}_{\rm R}. \quad (10)$$

Thus Bowen's (1988) models predict indeed a very steep increase of mass loss with increasing luminosity for a given mass. We have used this relation (10) along with evolutionary constraints to construct an AGB mass-loss formula. Therefore, we introduced a mass-dependent scaling function $\Gamma(M)$ in order to rewrite the relation above like

$$\dot{M} = \Gamma(M) \cdot L^{2.7} \cdot \dot{M}_{\rm R}. \quad (11)$$

Taking now into account that the Reimers formula is still giving reasonable rates at the beginning of the AGB and that Mira-like stars should have periods of, say, more than 100 days, we set as a condition for the transition between a Reimers and a Bowen-like mass loss

$$\dot{M}(P_0 = 100\,{\rm d}) = \dot{M}_{\rm R} = \dot{M}_{\rm B}, \quad (12)$$

which can be used to determine the scaling function Γ. By means of (7) and the conditions of Bowen's standard model the luminosity $L_{\rm scal}$ at this transition point can be calculated to be:

$$\log L_{\rm scal} = 3.08 + 0.78 \log M. \quad (13)$$

Below this luminosity the mass-loss rate should be calculated according to $\dot{M}_{\rm R}$, above to $\dot{M}_{\rm B}$. With (11) and (12) we immediately can determine Γ

$$\Gamma = \frac{1}{L_{\rm scal}^{2.7}}, \quad (14)$$

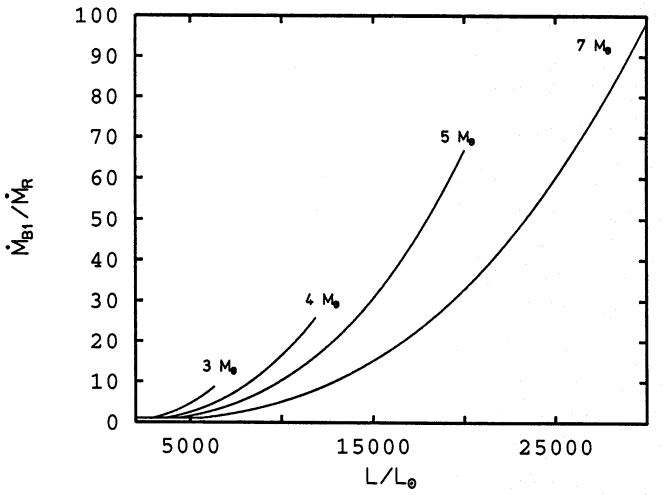

Fig. 2. The ratio $\dot{M}_{B1}/\dot{M}_R$ as a function of the stellar luminosity for inital masses of 3, 4, 5 and $7M_\odot$. At the respective tip of the AGB mass losses amount up to $\approx 10^{-4} M_\odot$ yrs^{-1}

and finally got by means of (13) and (14)

$$\Gamma = 4.83 \cdot 10^{-9} M^{-2.1}. \qquad (15)$$

The stellar mass M at the transition point in (13) and (15) can be approximated by the initial mass M_{ZAMS}, at least for models with $M_{ZAMS} > 2M_\odot$ whose integrated mass loss is only small until they reached $P_0 = 100$ d.

Thus, we finally got the following mass-loss formula for $P_0 > 100$ d:

$$\dot{M}_{B1} = 4.83 \cdot 10^{-9} M_{ZAMS}^{-2.1} \cdot L^{2.7} \cdot \dot{M}_R \qquad [M_\odot/\mathrm{yr}] \qquad (16)$$

Please note that the expression (16) is not a fit to the data of Bowen (1988) but does reflect the increase of mass loss with increasing luminosity as predicted by those dynamical calculations. The absolute values of the mass-loss rates depend on the introduced scaling. At a given luminosity mass losses are smaller for larger masses (cf. Fig. 2).

In order to simulate an even steeper increase of the mass-loss rates we additionally set, somewhat arbitrarily, the stellar mass M in (15) equal to the actual total mass leading to

$$\dot{M}_{B2} = 4.83 \cdot 10^{-9} M^{-2.1} \cdot L^{2.7} \cdot \dot{M}_R \qquad [M_\odot/\mathrm{yr}] \qquad (17)$$

Figure 2 illustrates the increase of $\dot{M}_{B1}$ in units of the corresponding Reimers rates as a function of the luminosity for inital masses of 3, 4, 5 and $7M_\odot$. The ratio $\dot{M}_{B1}/\dot{M}_R$ increases continously while the model climbs up the AGB. At the tip of the AGB ratios of 10...100 are reached providing easily a superwind of $\approx 10^{-4} M_\odot$/yr. Sequences with $\dot{M}_{B2}$ will have a mass-loss evolution which is even more steeper because the decreasing total mass additionally accelerates mass loss.

3.2.2. Model results

Starting at the base of the AGB we have calculated several sequences with the mass-loss formulae derived in the previous section. We used the Reimers law until a pulsational period of $P_0 = 100$ d was reached. For $P_0 > 100$d we introduced a Bowen-like mass-loss according to (16) and (17), resp. ($\dot{M}_{B1}$: 1, 3, 4, 5, $7M_\odot$; $\dot{M}_{B2}$: 3, $5M_\odot$). The particular choice of the scaling luminosity guarantees a smooth transition from the preceeding mass-loss law to the Bowen-like rates.

However, as mentioned above the $1M_\odot$ model lost already on the RGB 30% of its initial mass. Due to the small envelope mass with which the model entered the AGB, mass loss led to a termination of the AGB evolution at $M_H = 0.524M_\odot$ immediately before reaching the TP-AGB. At this point P_0 was still below 100 d so that the transition to a Bowen-like mass-loss was not reached, too. Therefore, the largest mass loss encountered was only $10^{-7} M_\odot$/yr.

The core mass at the first thermal pulse, $M_H(1)$, vs. the initial mass is given in Fig. 3 (cf. Lattanzio 1986; Boothroyd & Sackmann 1988). If a star reaches the TP-AGB its minimum final mass is, of course, at least as large as $M_H(1)$. Whereas the course of $M_H(1)$ varies only slightly for low initial masses it steeply increases for $M_{ZAMS} \approx 3.5M_\odot$ and flattens out for $M_{ZAMS} > 6M_\odot$. Since the core growth ΔM_H per pulse decreases from several $10^{-3} M_\odot$ for a $0.6M_\odot$ core to $\approx 10^{-3} M_\odot$ for a $0.9M_\odot$ core (more details will be given in Blöcker 1994b) one can expect that strongly increasing mass-loss rates will lead to a similarly shaped initial-final mass relation because they allow only a moderate number of thermal pulses (e.g. 15 to 20) to occur. For a further discussion of the mass loss on the TP-AGB and its connection to the initial-final relation see Mazzitelli (1989) and Weidemann (1993).

Table 1 gives the inital and final masses as well as the lifetimes on the E- and TP-AGB and the total number of thermal pulses for the different sequences whereas Fig. 4 shows the final versus the initial masses. The sequences calculated with $\dot{M}_{B1}$ or $\dot{M}_{B2}$ give combinations of initial and final masses which are consistent with the initial-final mass relationship of Weidemann (1987) (cf. Fig. 4). Indeed, one can recover the shape of the $M_H(1)$ vs. M_{ZAMS} relation for $\dot{M}_{B1}$. Correspondingly, the total number of thermal pulses is lowest for an initial mass of $5M_\odot$ due to the interplay of $\dot{M}$, $M_H(1)$ and ΔM_H.

The differences of the final masses are only noticable for low-mass sequences: For $M_{ZAMS} = 3M_\odot$ one gets 0.605 and $0.625M_\odot$, resp., corresponding to 17 and 20 thermal pulses. For larger initial masses ($> 5M_\odot$) the differences are smaller than 1%. Since for $M > 2M_\odot$ the major mass loss takes place on the TP-AGB the influence of these different AGB mass-loss laws on the final mass becomes smaller for larger initial masses.

We have also calculated three AGB sequences (3, 5 and $7M_\odot$) with the mass-loss formula of Baud & Habing (1983). The evolution of the $3M_\odot$ star led to a final mass of $0.814M_\odot$ which is not consistent with observed initial-final mass relationships (cf. Fig. 4). Obviously, the increase of the mass-loss rates is too slow to remove enough mass in a reasonable time. Therefore, larger mass-loss rates (dependent on the envelope mass) are only reached very late. Due to the slow increase of this rate with increasing luminosity the duration of the TP-AGB evolution is quite long and many thermal pulses can occur, namely

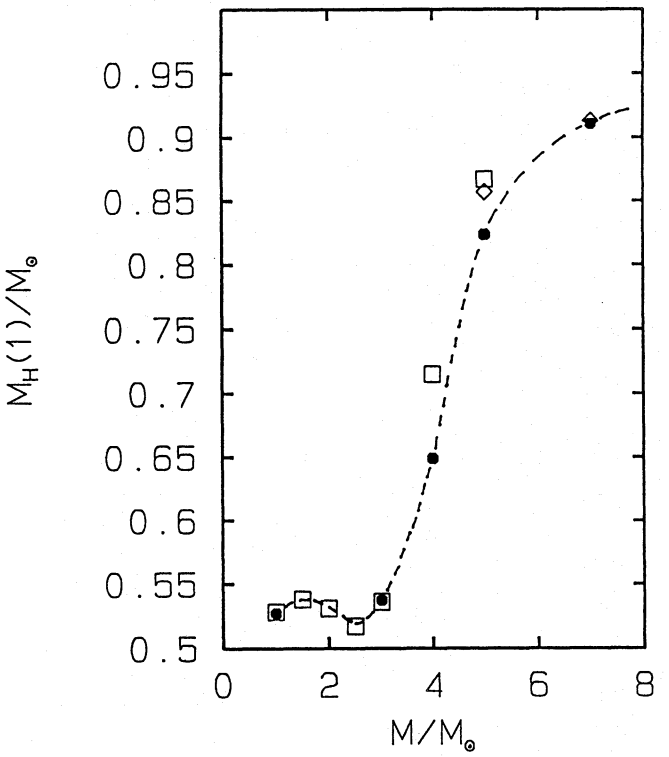

Fig. 3. Mass at the first thermal pulse vs. initial mass. Our models are indicated by filled circles. The results of Lattanzio (1986) [squares, Y=0.2] and of Becker & Iben (1980) [rhombs, Y=0.2] are also given

Table 1. Some properties of the models: initial mass, core mass at the tip of the AGB (≈ final mass), lifetime on the E-AGB and TP-AGB, total number of thermal pulses and the used mass-loss law. The symbols B1 and B2 refer to Bowen-like mass-loss rates given by (16) and (17), resp., R to Reimers (1975), BH to Baud & Habing (1983) and SP to a special treatment of mass-loss introduced to a get remnants of specified mass ($0.836M_\odot$, $0.94M_\odot$; see text). The open circles indicate those sequences whose AGB evolution have been completed and the filled circles those for which also the post-AGB evolution has been calculated. The asteriks refer to the sequences whose AGB evolution is still unfinished (see text), the given properties correspond to the last calculated models

$\frac{M_{ZAMS}}{M_\odot}$	$\frac{M_H}{M_\odot}$	$\frac{t_{E-AGB}}{yrs}$	$\frac{t_{TP-AGB}}{yrs}$	N_{TP}	$\dot{M}$	
1	0.529	$4.46 \cdot 10^7$	/	/	R	•
3	0.605	$6.96 \cdot 10^7$	$1.62 \cdot 10^6$	17	B2	•
	0.625		$1.87 \cdot 10^6$	20	B1	•
	0.814		$3.18 \cdot 10^6$	74	BH	○
	0.836		$3.26 \cdot 10^6$	86	SP	•
4	0.696	$1.98 \cdot 10^7$	$4.54 \cdot 10^5$	15	B1	•
5	0.828	$8.29 \cdot 10^6$	$2.89 \cdot 10^4$	5	B2	○
	0.836		$5.79 \cdot 10^4$	9	B1	•
	0.889		$2.83 \cdot 10^5$	46	BH	*
7	0.925	$1.71 \cdot 10^6$	$3.63 \cdot 10^4$	15	B1	○
	0.940		$8.50 \cdot 10^4$	31	SP	•
	0.947		$1.04 \cdot 10^5$	38	BH	*

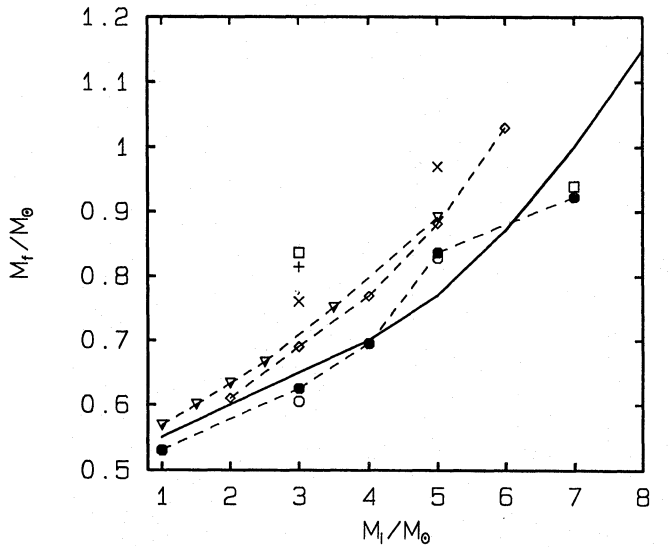

Fig. 4. Final mass vs. initial mass for different mass loss histories on the AGB. The solid line is the initial-final mass relationship of Weidemann (1987). The symbols mean:
• $\dot{M}_{B1}$ ○ $\dot{M}_{B2}$ + $\dot{M}_{BH}$ ◇ $\dot{M}_{BVK}$
× $\dot{M}_{VK}$ □ sp. ▽ $\dot{M}_{VW}$

74 in the case of the $3M_\odot$ sequence, corresponding to 120000 stellar models. Since the mass-loss rates are quite low the calculations for 5 and $7M_\odot$ have not been finished yet. Up to now these models have suffered from 46 and 38 thermal pulses, resp., but their present masses are still 4.3 and $6.7M_\odot$, resp.

In order to get two massive AGB remnants with the same final mass but different history, i.e. initial mass, we split the $3M_\odot$ sequence with $\dot{M} = \dot{M}_{BH}$ setting for that purpose $\dot{M} = 0$ after pulse No. 62 when $(M, M_H) = (1.67M_\odot, 0.784M_\odot)$. After additional 24 pulses $M_H = 0.836M_\odot$ was reached. A well-timed beginning of a constant mass-loss rate of $\dot{M} = 5 \cdot 10^{-4}\, M_\odot/yr$ guaranteed that this was the final mass, too. Looking at Fig. 4 one sees that this remnant mass is, of course, definitely too large for a progenitor of $3M_\odot$. The same is true for the more massive remnants of Wood & Faulkner (1986) which all belong to a progenitor of $2M_\odot$.

The different histories (M_{ZAMS} = 3 and $5M_\odot$) of these remnants of equal mass ($0.836M_\odot$) will have severe consequences for the fading timescales of the central-star evolution (see Sect. 3.2.5 and Blöcker 1993b).

We have also split the $7M_\odot$ sequence with $\dot{M} = \dot{M}_{BH}$ in order to get a massive remnant of $0.94M_\odot$ and to investigate the influence of different mass-loss laws on hot bottom burning (see Sect. 3.2.4). This was done by introducing a constant rate

of $\dot{M} = 4 \cdot 10^{-4}\, M_\odot$/yr at pulse No. 26. The AGB evolution terminated 5 pulses later.

Finally, the comparison of the different mass-loss descriptions discussed in Sect. 3.2.1 with the empirical initial-final mass relation of Weidemann (1987) clearly shows that only a few formulae yield consistent remnant masses. The results of Bryan et al. (1990) and of Vassiliadis & Wood (1993) agree well with the observed relation for lower initial masses. Concerning larger initial masses, e.g. $5M_\odot$, the remnant masses are up to $\approx 0.1M_\odot$ above Weidemann's (1987) relation. The initial-final mass combinations provided by $\dot{M}_{\rm B1}$ seem to be consistent with the empirical relation over the whole mass range.

3.2.3. Mass-loss modulations by thermal pulses

During one thermal-pulse cycle the star does not only suffer from strong variations of its interior luminosity contributions (e.g. of the hydrogen and helium burning shell, gravothermal contributions) but also of its surface parameters like radius, effective temperature and luminosity. Figure 5 illustrates the variations of these parameters for initial masses of 3, 4, 5 and $7M_\odot$ along the $10^{\rm th}$ pulse cycle as a function of the cycle phase ϕ. The phase ϕ is defined as the fraction of the time span between two subsequent pulses (with respect to the peak luminosity of the helium burning shell).

Whereas the effective temperature shows only slight changes, the surface luminosity as well as the radius are considerably affected by the occurrence of a thermal pulse. Hence, all quantities depending on these parameters, like mass-loss rates or pulsational periods, will also vary during a pulse cylce. The strength of the mass-loss variations depend on the used mass-loss law. This is shown in Fig. 6 for $M_{\rm ZAMS} = 3M_\odot$ and two mass-loss laws ($\dot{M}_{\rm B1}$ and $\dot{M}_{\rm BH}$) during the $10^{\rm th}$ pulse cycle. Since $\dot{M}_{\rm B1} \sim L^{3.7}$ the Bowen-like mass-loss rate varies by ≈ 2 orders of magnitude whereas $\dot{M}_{\rm BH}$ ($\sim L$) changes by only one order of magnitude. The formula given by Vassiliadis & Wood (1993) also provides strong mass-loss modulations.

Thus, thermal pulses are leading to modulations, or short interruptions, of the continuously increasing AGB mass-loss rates. These modulations seem to be responsible for the loops in the IRAS two clour diagram which have been observed for C stars as well as for M stars (cf. Olofsson et al. 1990; Van der Veen & Habing 1988; Kwok et al. 1989; Zijlstra et al. 1992).

In order to be consistent with the observations a sufficiently strong modulation of the mass-loss rates is required (e.g. in the range from 10^{-5} to $10^{-7}M_\odot$/yr). Szczerba & Marten (1993b) have performed hydrodynamical dust shell calculations based on our $3M_\odot$ sequence with $\dot{M}_{\rm B1}$ and reached a reasonable agreement with the observations. The exact shape of the loops is determined by the thermal-pulse cycle and the mass-loss variations and additionally by dynamical effects and the dust shell chemistry.

The whole temporal mass-loss evolution along the AGB for the 3, 4, 5 and $7M_\odot$ sequence calculated with $\dot{M}_{\rm B1}$ is shown in Fig. 7. Due the strong luminosity dependence $\dot{M}_{\rm B1}$ rises steeply during the AGB evolution reaching up to $\approx 10^{-4}M_\odot$/yr at the

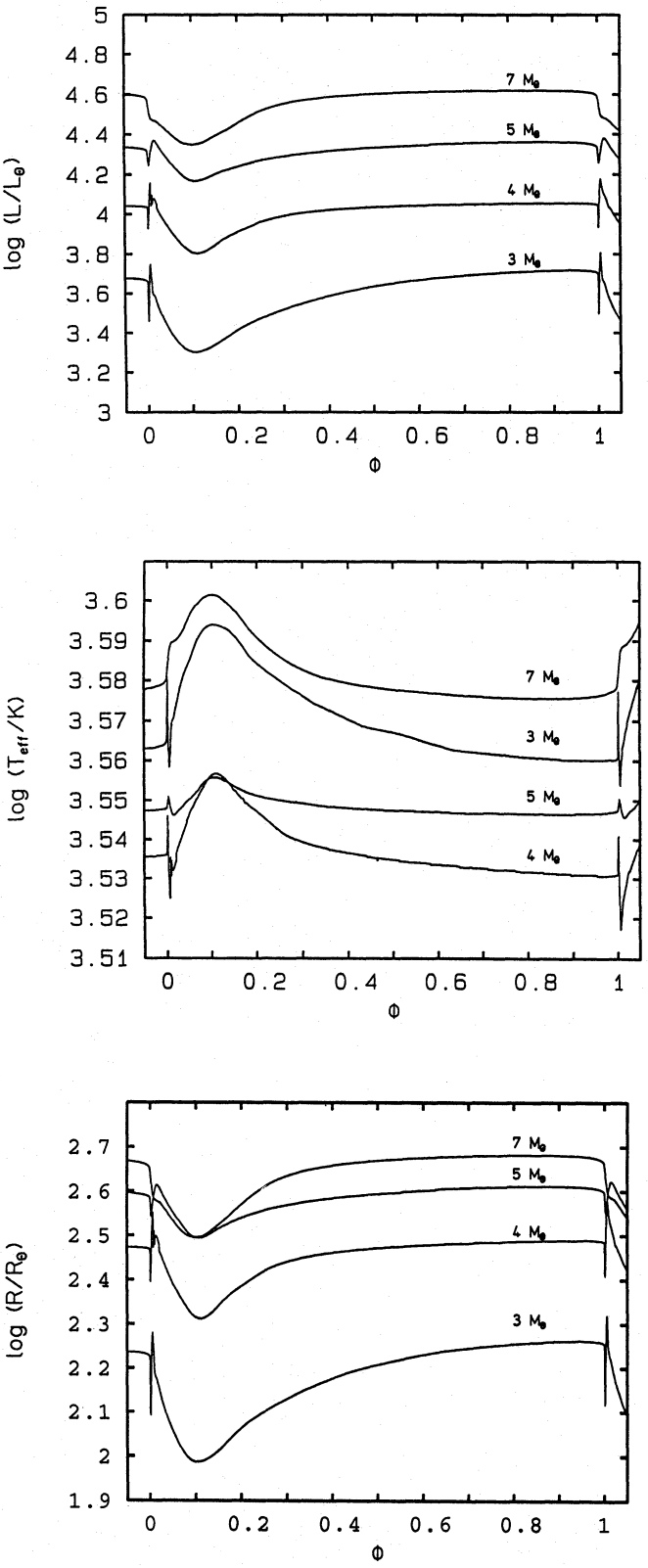

Fig. 5. Surface luminosity (upper panel), effective temperature (middle panel) and stellar radius (lower panel) as a function of the thermal-pulse cycle ϕ for the $10^{\rm th}$ pulse of a 3, 4, 5 and $7M_\odot$ sequence

tip of the AGB. The models are suffering from 20, 15, 9 and 15 thermal pulses, resp. After the termination of the AGB evolution the high AGB mass loss rates were smoothly reduced. This reduction has been conducted between pulsational periods of 100 and 50 d in such a way that the Reimers rate was reached at $P_0 = 50$ d. The latter point defines our zero point of the central star evolution and corresponds to $t = 0$ in the respective figures (see Blöcker 1994a for more details).

3.2.4. Mass loss and hot bottom burning

In this section we discuss the connection between mass loss and hot bottom burning. A more detailed discussion of hot bottom burning models will given in a forthcoming part of this series.

During the evolution along the AGB the envelope convection gets more and more extended downwards due to the increasing radiation pressure. In the case of large initial masses ($> 5M_\odot$) and large core masses ($> 0.8M_\odot$) the envelope convection can reach and penetrate the hydrogen burning shell. This has consequences concerning nucleosynthesis and the core-mass luminosity relation. The temperature at the base of the convective shell strongly increases ("hot bottom burning") and the models become very luminous: They do not follow any longer the classical core-mass luminosity relation of Paczyński (1970) as has been shown by Blöcker & Schönberner (1991) and confirmed by Lattanzio (1992) and Boothroyd & Sackmann (1992). The evolution of the temperature at the base of the convective envelope is shown in Fig. 8 for a $7M_\odot$ model ($\dot{M} = \dot{M}_{\rm BH}, \alpha = 2$). Already on the E-AGB the convective envelope cuts into the hydrogen burning shell. During the thermal-pulse phase the temperatures steeply increase, reaching $80 \cdot 10^6$ K and more. At the 30$^{\rm th}$ pulse almost 50% of the luminosity is produced within the convective envelope. The production of ^{7}Li and its mixing to the surface (e.g. Scalo et al. 1975; Blöcker & Schönberner 1991; Sackmann & Boothroyd 1992) as well the transformation of a C star into a N-rich S star (e.g. Iben 1975; Renzini & Voli 1981; Boothroyd et al. 1993) is closely connected with the occurence of hot bottom burning.

Figure 9 shows the luminosity evolution as a function of the envelope mass for two different mass-loss histories on the AGB (Blöcker 1993a). In one case we took the first 26 thermal pulses of the $7M_\odot$ sequence with $\dot{M}_{\rm BH}$ and artificially switched on a "superwind" of $4 \cdot 10^{-4} M_\odot$/yr leading to a termination of the AGB evolution after only five additional thermal pulses. During the first part the model evolves rapidly to higher luminosities at virtually constant mass. At the 20th thermal pulse the model breaks through the classical AGB limit of $\approx 52000L_\odot$. However, with decreasing envelope mass due to the invoked large mass loss the deviations from the core-mass luminosity relation decrease, too, and hence the strength of hot bottom burning. This is due to the shrinking extent of the convective envelope. At the end of the AGB evolution, core and envelope are decoupled again due to appearence of the radiative buffer layer between them, and the model finally obeys again the core-mass luminosity relationship before it leaves the AGB.

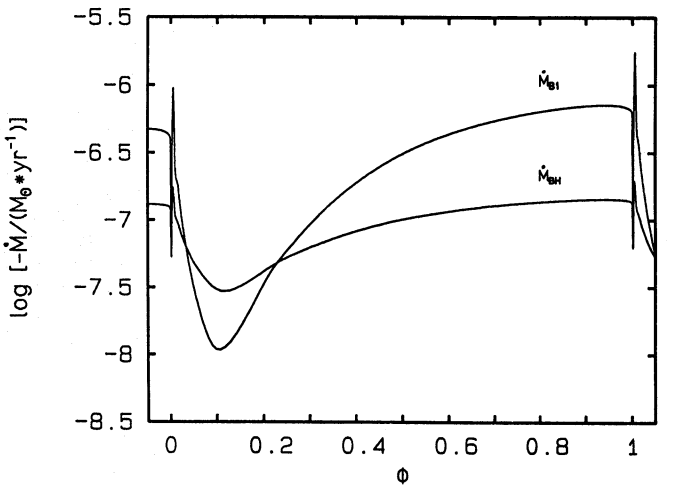

Fig. 6. The mass-loss rates $\dot{M}_{\rm BI}$ and $\dot{M}_{\rm BH}$ as function of the thermal-pulse cycle ϕ for the 10$^{\rm th}$ pulse of a $3M_\odot$ sequence

The second sequence was calculated with the more realistic rate $\dot{M}_{\rm BI}$, resulting in 15 thermal pulses. Due to the faster reduction of the envelope mass the models did not become as luminous as in the previous case. However, the deviations from the classical relation still amount to $\approx 10000L_\odot$. The maximum temperature reached at the base of the convective envelope is $75 \cdot 10^6$ K. Thus, if hot bottom is efficient it cannot be prevented even by high mass loss rates!

The close connection between mass loss and nucleosynthesis for hot bottom burning models can be summarized as follows: On the one hand the temperature at the base of the convective envelope is uniquely correlated with the luminosity, i.e. the higher the luminosity the higher is the base temperature (cf. Fig. 8). On the other hand, the luminosity is also determined by the present envelope mass, i.e. by mass-loss history (cf. Fig. 9). For sufficiently small envelope masses the luminosity approaches the prediction of the core-mass luminosity relation. Consequently, there exists for a given envelope mass and mass-loss law a maximum luminosity with a concomitant maximum base temperature. Furthermore, the envelope mass and its variation with time determines the dilution of the material mixed to the surface which will be important for surface abundance predictions and the yield in general.

3.2.5. Mass loss and internal structure

Paczyński (1970) has shown that the evolutionary lines of degenerate cores belonging to different initial masses do converge in the density-temperature plane. Only if the evolutionary lines have merged into such a "limiting line" the corresponding cores have the same internal, i.e. thermomechanical, structure implying an equal post-AGB evolution. Figure 10 shows the evolution of the respective central values for different initial masses.

The wiggles which can be seen along the TP-AGB correspond to the response of the core's center to the occurence of

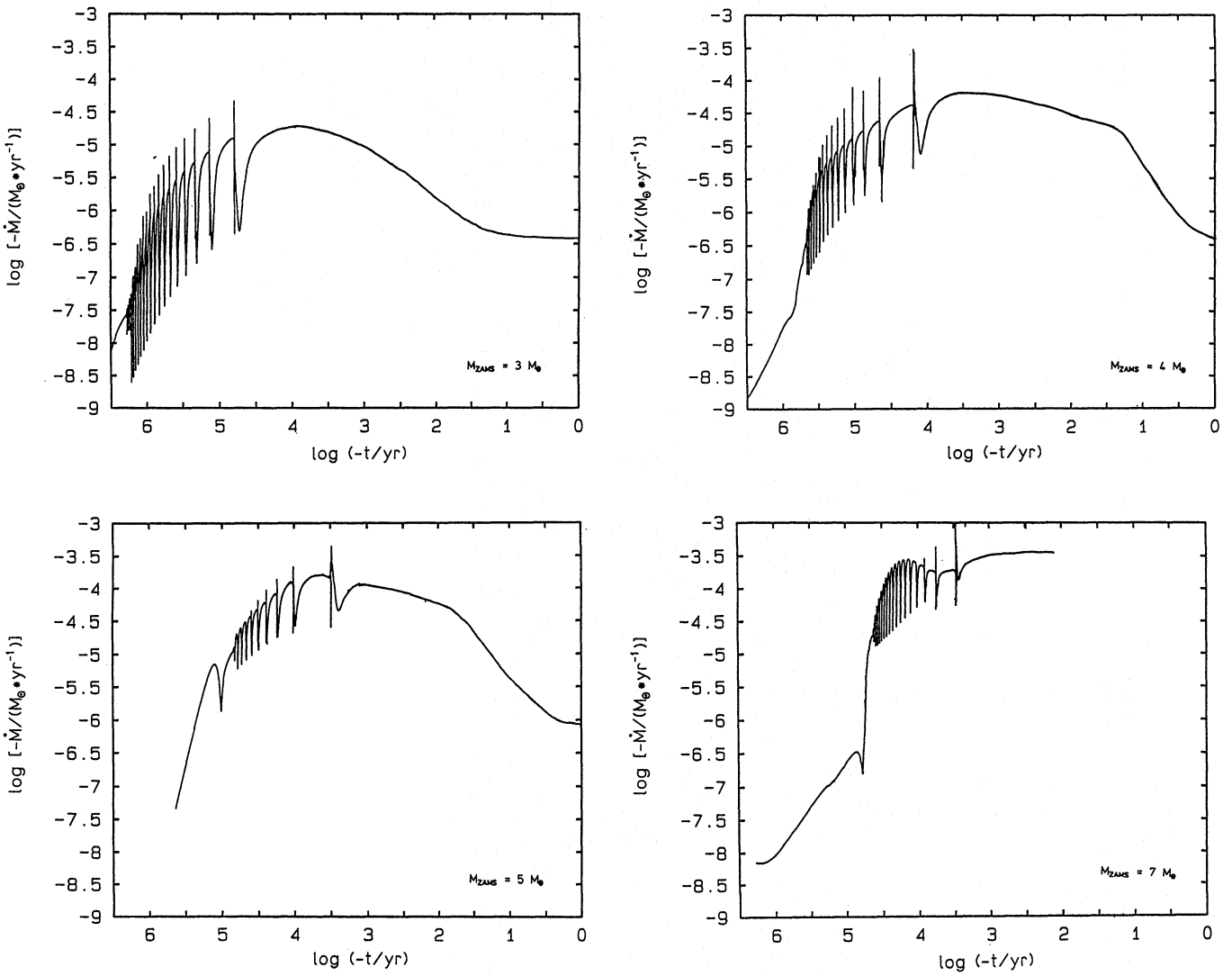

Fig. 7. Temporal evolution of the mass-loss rate $\dot{M}_{\rm B1}$ along the AGB for a 3, 4, 5 and $7M_\odot$ sequence (20, 15, 9 and 15 thermal pulses). The point $t = 0$ refers to the zero point of the central star evolution corresponding to $P_0 = 50$ d

thermal pulses. The size of the wiggles depends on the pulse strength as well as on the respective equation of state.

The dashed line indicates the tip of the AGB for the sequences calculated with $\dot{M}_{\rm B1}$. Obviously, the consideration of mass loss terminates the AGB evolution far before the point of convergence. Even in the case of equal remnant masses (here $0.836M_\odot$) the internal structure can be quite different (cf. Fig. 10).

Some relevant data at the tip of the AGB concerning the $0.836M_\odot$ remnants in comparison with one of $0.605M_\odot$ is given in Table 2. The massive remnant belonging to the $3M_\odot$ progenitor is due to its long AGB evolution more compact and cooler, and thus more degenerate, in the interior than the one from the $5M_\odot$ progenitor. Due to this different thermomechanical structure the post-AGB evolution can be expected to be different, too!

This important point is emphasized by the evolution of the gravothermal luminosity $L_{\rm g}$ and the neutrino losses L_ν along the AGB which is shown in Fig. 11 as a function of the core mass. Whereas both luminosity contributions which are almost totally determined by the core (see Fig. 12 for an example) increase with increasing core mass (or time) for an initial mass of $3M_\odot$ the reverse is true for initial masses of 5 and $7M_\odot$. As to be expected, there seems to be again a common evolutionary line but like in the density-temperature plane such a convergence is prevented in our cases by mass-loss. Thus, even massive cores of equal mass have totally different gravothermal energy contributions and neutrino losses due to their different internal structures. For example, the remnant with a $5M_\odot$ parent star has a gravothermal luminosity $L_{\rm g}$ nearly twice as large as the cool and old one of the same mass evolving from a $3M_\odot$ progenitor ($1500L_\odot$ instead of $830L_\odot$).

Table 2. Some properties of the models: initial mass, core mass at the tip of the AGB (≈ final mass), total lifetime on the AGB, total number of thermal pulses and central values of density and temperature as well as the radius of the hydrogen burning shell

M_{ZAMS}	M_H	t_{AGB}	N_{TP}	$\log\left(\frac{\rho_c}{gcm^{-3}}\right)$	$\log\left(\frac{T_c}{K}\right)$	R_H
$3M_\odot$	$0.605M_\odot$	$7.12 \cdot 10^7$ yrs	17	6.384	7.947	$0.0253R_\odot$
	$0.836M_\odot$	$7.52 \cdot 10^7$ yrs	86	7.005	7.932	$0.0163R_\odot$
$5M_\odot$	$0.836M_\odot$	$8.35 \cdot 10^6$ yrs	9	6.916	8.092	$0.0183R_\odot$

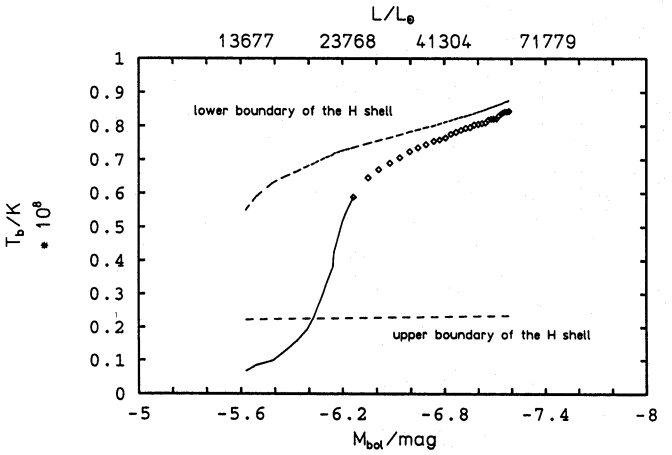

Fig. 8. Temperature at the base of the convective envelope vs. M_{bol} for a $7M_\odot$ AGB model with $\alpha = 2$. Mass loss was calculated according to Baud & Habing (1983). The solid line shows the base temperature evolution on the E-AGB from the re-ignition of the hydrogen shell till the 1st thermal pulse. Rhombs refer to our models immediate before pulse No. 1 till No. 38

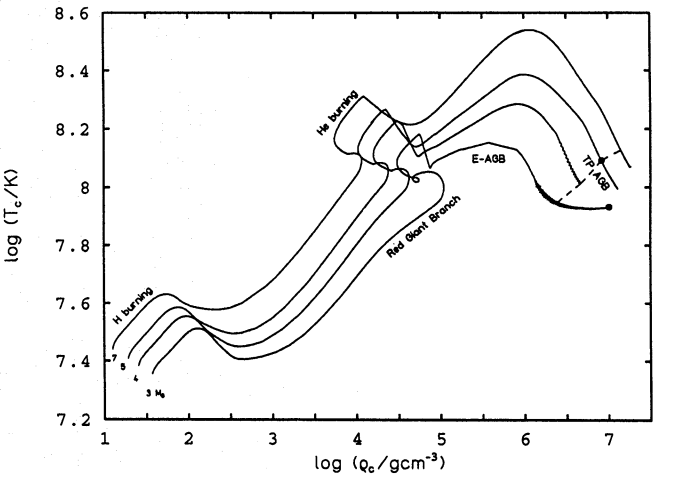

Fig. 10. Evolution of the central values of density and temperature for different initial masses. The dashed line indicates the tip of the AGB for sequences calculated with $\dot{M}_{B1}$, the filled dots refer to massive remnants of $0.836M_\odot$

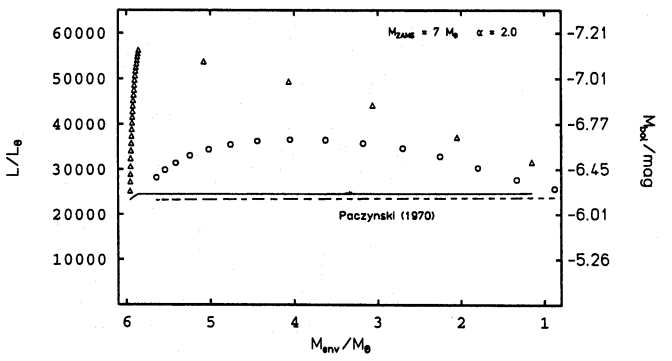

Fig. 9. Luminosity vs. envelope mass M_{env} for a $7M_\odot$ AGB model with $\alpha = 2$. Triangles refer to a sequence calculated with $\dot{M}_{BH}$ (26 thermal pulses) and an artifically invoked "superwind" of $\dot{M} = 4 \cdot 10^{-4} M_\odot$/yr (5 thermal pulses). The circles denote the corresponding evolution with the Bowen-like mas-loss $\dot{M}_{B1}$ (15 thermal pulses). The solid and dashed line indicate what is to be expected according to Paczyński (1970), the differences between the two lines are due to slightly different core masses

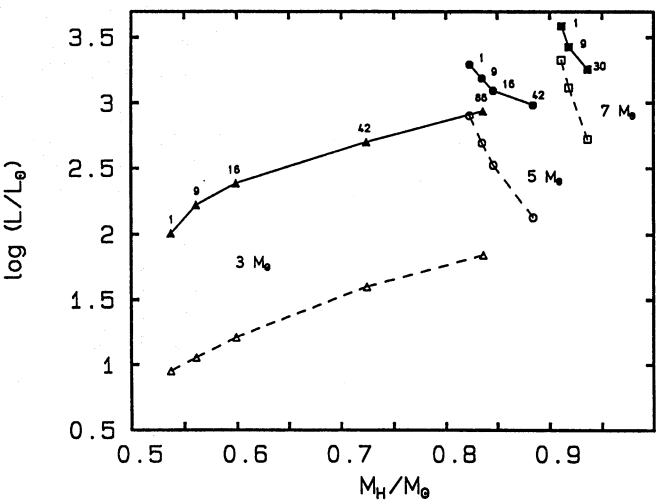

Fig. 11. Evolution of L_g (filled symbols) and L_ν (open symbols) along the AGB for three initial masses. The numbers denote selected thermal pulses ($\phi = 0.5$)

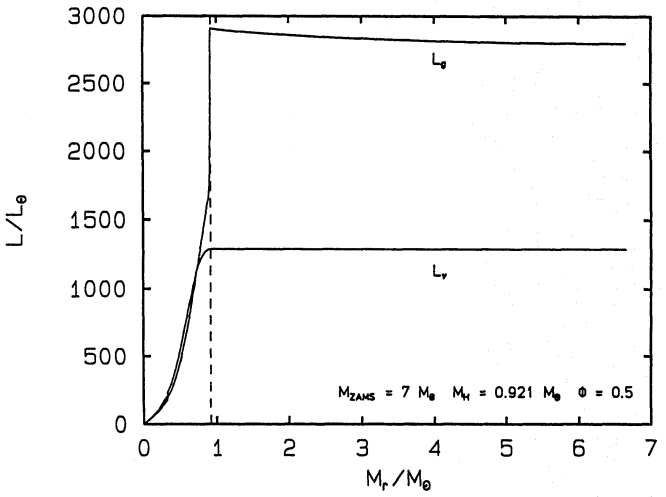

Fig. 12. L_g and L_ν as a function of M_r (mass inside radius r). The model belongs to the 10th pulse cylce at $\phi = 0.5$ of a $7M_\odot$ sequence with $\dot{M} = \dot{M}_{BH}$

4. Conclusions

Our calculations indicate that mass loss is one of the most important parameters of the late stellar evolution because it determines not only the final mass reached at the tip of the AGB but also the internal structure and nucleosynthesis.

We have derived a mass-loss formula based on dynamical calculations for atmospheres of Mira-like stars by Bowen (1988). The results of our calculations performed with this formula are consistent with the empirical initial-final mass relationship of Weidemann (1987) over the whole mass range.

A discussion and comparison of other AGB mass-loss formulae like those of Volk & Kwok (1988), Baud & Habing (1983), and Bedijn (1987) show that these descriptions yield too high final masses and, thus, are not consistent with the initial-final mass relationship whereas the results of Bryan et al. (1990) and Vassiliadis & Wood (1993) agree much better with the empirical relation.

One common feature of all mass-loss formulae considered so far is that they do not depend on metallicity. However, Bowen's (1988) calculations clearly indicate that mass loss can decrease strongly (≈ 2 orders of magnitude) if no dust is considered. Furthermore, the most luminous galactic OH/IR objects and the most luminous long period variables of the Magellanic Clouds have approximately the same periods at comparable luminosities. However, the OH/IR objects are surrounded by thick circumstellar shells and are visible only in the infrared whereas the LPVs are optical sources and, thus, must suffer from much lower mass-loss rates (Iben 1994). Work is in progress to expand our formula also to models without dust, i.e. to take explicitly metallicity effects into account.

Besides giving an "accelerated" increase during evolution and producing consistency with initial-final mass relations, AGB mass-loss rates must also show large variations during the thermal-pulse cycles in order to recover the observed loops in the IRAS two colour diagram. Dust shell calculations of Szczerba & Marten (1993b) based on our mass-loss rates and thermal-pulse cycles indicate that the luminosity dependence of the mass-loss rates predicted by Bowen's (1988) models provides sufficiently strong modulations as compared with the observations. In turn, such hydrodynamical dust shell calculations in connection with consistent stellar evolution models may provide further constraints for the determination of mass-loss laws.

A realistic consideration of mass loss is also important for the investigation of hot bottom burning models. On the one hand, hot bottom burning cannot be prevented even by high mass-loss rates if it is sufficiently strong (like in the case of our $7M_\odot$ sequence). However, the deviations from the classical core-mass luminosity relation (Paczyński 1970) are also a function of the actual envelope masses and, thus, efficient mass-loss rates weaken the overluminosity (cf. Fig. 9). Hence, mass loss determines also the maximum temperature reached at the bottom of the convective envelope which, in turn, is an unique function of the luminosity. Obviously, the nucleosynthesis connected with hot bottom burning may also strongly be influenced by the used mass-loss law since it depends on the combination of initial, core and envelope mass.

Finally, the AGB mass-loss history lays the foundation for the time scales of the subsequent evolutionary stages until the white dwarf regime is reached. This is simply due to the fact that the internal structure reached at the tip of the AGB depends on the the lifetime on the AGB and, thus, on mass loss. As can be seen in the density-temperature plane (Fig. 10) mass loss prevents the convergence of the evolutionary lines, and even remnants of equal mass can have a completely different thermomechanical structure. This is reflected by the evolution of the gravothermal luminosity and the neutrino losses along the AGB (Fig. 11). During the evolution the core interiors get cooler and more contracted, and, thus, more degenerate. After leaving the AGB and the exhaustion of nuclear shell burning the fading time scales depend on the mean degeneracy. The higher the degeneracy, the more energy which is released by contraction is used up to raise the Fermi energy of the electrons and is not available any longer for the thermal content of the star. Thus, for a given initial mass the fading is faster the older the remnant. In turn, for a given remnant mass the fading will be faster the lower the progenitor mass. A detailed discussion of the post-AGB evolution and its connection to the preceding AGB history will be the subject of the second part of this series.

Acknowledgements. I wish to thank Prof. D. Schönberner for his careful reading of the manuscript and many valuable suggestions. Funding by the Deutsche Forschungsgemeinschaft (Scho 394/1-1 and 1-2) is acknowledged. Most of the calculations presented here have been performed at the Institut für Astronomie und Astrophysik in Kiel. The computations were conducted on the CRAY-XMP and -YMP of the Rechenzentrum der Universität Kiel.

References

Adams, W.S., McCormack, E., 1935, ApJ 81, 119
Baud, B., Habing, H.J.: 1983, A&A 127, 73

Baud, B., Habing, H.J., Matthews, H.E., Winnberg, A., 1979, A&AS 35,179
Becker, S.A., Iben, I. Jr., 1980, ApJ 237, 111
Bedijn, P.J., 1987, A&A 186, 136
Blöcker, T.: 1989, Diploma thesis, University of Kiel
Blöcker, T.: 1993a, PhD thesis, University of Kiel
Blöcker, T.: 1993b, in *White Dwarfs: Advances in Observation and Theory*, ed. M.A. Barstow, NATO ASI Series C, Kluwer, Dordrecht, p. 59
Blöcker, T.: 1994a, A&A, in press
Blöcker, T.: 1994b, A&A, in preparation
Blöcker, T., Schönberner, D., 1990, A&A 240, L11
Blöcker, T., Schönberner, D., 1991, A&A 244, L43
Böhm-Vitense, E., 1958, Z.Astrophys. 46, 108
Boothroyd, A.D., Sackmann, I.-J., 1988, ApJ 328, 653
Boothroyd, A.D., Sackmann, I.-J., 1992, ApJ 393, L21
Boothroyd, A.D., Sackmann, I.-J., Ahern, S.C., 1993, ApJ 416, 762
Bowen, G.H., 1988, ApJ 329, 299
Bowers, P.F., 1985, in *Mass Loss in Red Giants*, eds. M. Morris & B. Zuckermann, Reidel, Dordrecht
Bryan, G.L., Volk, K., Kwok, S., 1990, ApJ 365, 301
Canuto, V.M., 1970, ApJ 159, 641
Cox, A.N., Stewart, J.N., 1970, ApJS 19, 243
Deutsch, A.J., 1956, ApJ 123, 210
Habing, H.J., van der Veen, W., Geballe, T., 1987, in it Late Stages of Stellar Evolution, eds. S. Kwok und S.R. Pottasch, Dordrecht, Reidel, p.91
Hashimoto, O., Nakada, Y., Onaka, T., Tanabé, T., Kamijo, F., 1990, A&A 227, 465
Hubbard, W.B., Lampe, M., 1969, ApJS 163, 297
Iben, I. Jr., 1975, ApJ 196, 525
Iben, I. Jr., 1994, Physics Reports, in press
Iglesias, C.A., Rogers, F.J., Wilson, B., 1992, ApJ 397, 717
Johannsson, L.E.B., Anderson, B., Gross, M., Winnberg, A., 1977, A&AS 28, 199
Knapp, G.R., Morris, M., 1985, ApJ 292, 640
Kuiper, T.B.H., Knapp, G.R.,Knapp, S.L., Brown, R.L., 1976, ApJ 204, 408
Kwok, S., Volk, K. M., Chan, S. J., 1989 in *Evolution of Peculiar Red Giant Stars*, IAU Coll. 106, eds. H.R. Johnson & B. Zuckermann, Cambridge University Press, p. 284
Lafon, J.-P.J., Berruyer, N., 1991, A&A Rev 2, 249
Lattanzio, J.C., 1986, ApJ 311, 708
Lattanzio, J.C., 1992, Proc. Astron. Soc. Austr. 10, 120
Maeder, A., Meynet, G., 1989, A&A 210, 155
Mazzitelli, I., 1989, in *White Dwarfs*, Lecture Notes in Physics Vol. 328, ed. G. Wegner, Springer, Berlin
Neugebauer, G., Leighton, R.B., 1969, Two Micron Sky Survey, NASA SP-3047
Netzer, N., Elitzur, M., 1993, ApJ 410, 701
Olnon, F. M., Baud, B., Habing H.J., de Jong, T., Harris, S., Pottasch, S.R., 1984, ApJ 278, L41
Olofsson, H., Carlström, U., Eriksson, K., Gustafsson, B., Willson, L.A., 1990, A&A 230, L13
Ostlie, D., Cox, A.N.: 1986, ApJ 311, 864
Paczyński, B., 1970, Acta Astron. 20, 47
Price, S.D., Walker, R.G., 1976, The AFGL Four Colour Infrared Sky Survey, AFGL TR-76-0208
Reimers, D., 1975, "Problems in Stellar Atmospheres and Envelopes", B. Baschek, W.H. Kegel, G. Traving (eds.), Springer, Berlin, p. 229
Renzini, A., 1981, in *Physical Processes in Red Giants*, eds. I. Iben Jr., A. Reninzi, Reidel, Dordrecht, p. 481
Renzini, A., Voli, M., 1981, A&A 94, 175
Rogers, F.J., Iglesias, C.A., ApJS 79, 507
Rowan-Robinson, M., Lock, T.D., Walker, D.W., Harris, S., 1986, MNRAS 222, 273
Sackmann, I.-J., Boothroyd, A.I., 1992, ApJ 392, L71
Salpeter, E.E., 1974, ApJ 193, 585
Scalo, J.M., Despain, K.H., Ulrich, R.K., 1975, ApJ 196, 805
Schönberner, D., 1979, A&A 79, 108
Schönberner, D.: 1983, ApJ 272, 708
Szczerba, R., Marten H., 1993a, in *Mass loss on the AGB and Beyond*, ESO Conference and Workshop Proc. No. 46, p. 90
Szczerba, R., Marten H., 1993b, private communication
van der Veen, W.E.C.J., 1987, in it Late Stages of Stellar Evolution, eds. S. Kwok und S.R. Pottasch, Reidel, Dordrecht, p. 309
van der Veen, W.E.C.J., Habing, H.J., 1988, A&A 194, 125
van der Veen, W.E.C.J., Habing, H.J., Geballe, T.R., 1989, A&A 226, 108
Volk, K., Kwok, S., 1988, ApJ 331, 435
Vassiliadis, E., Wood, P.R., 1993, ApJ 413, 641
Weidemann, V.: 1987, A&A 188, 74
Weidemann, V., 1993, in *Mass loss on the AGB and Beyond*, ESO Conference and Workshop Proc. No. 46, p. 59
Weidemann, V., Koester, D., 1983, A&A 121, 77
Wood, P.R., 1990, in *From Miras to Planetary Nebulae: Which Path for Evolution?*, eds. M.O. Mennessier & A. Omont, Editions Frontieres, p.67
Wood, P.R., Faulkner, D.J., 1986, ApJ 307, 659
Woolf, N.J., Ney, E.P., 1969, ApJ 155, L181
Zijlstra, A.A., Loup, C., Waters, L.B.F.M., de Jong, T., 1992, A&A 265, L5

This article was processed by the author using Springer-Verlag LaTeX A&A style file version 3.